2008 IEEE International Conference on
Robotics and Automation
Pasadena, CA, USA, May 19-23, 2008

Static Lumped Parameter Model for Nested PZT Cellular Actuators with Exponential Strain Amplification Mechanisms

Jun Ueda, Thomas Secord, and H. Harry Asada

Abstract— **A static lumped parameter model is proposed for the design and analysis of nested piezoelectric cellular actuators with exponential strain amplification mechanisms. Piezoelectric ceramic material, such as Lead Zirconate Titanate (PZT), has large stress and bandwidth, but its extremely small strain, i.e. only 0.1%, has been a major bottleneck for broad applications. We have proposed a "nested rhombus" multi-layer mechanism for PZT actuators, which increases strain exponentially through its hierarchical cellular structure, for over 20% effective strain. To drive a large load, however, care must be taken in the design of the strain amplification structure. Through kinematic and static analysis this paper addresses how the output force and displacement are attenuated by the joint stiffness and beam compliance involved in the strain amplification mechanism. An insightful lumped parameter model is developed to quantify the performance degradation and facilitate design trade-offs. A prototype nested PZT cellular actuator that weighs only 15 g has produced 21% effective strain (2.49 mm displacement from 12 mm actuator length) and 1.7 N blocking force.**

I. Introduction

Piezoelectric ceramics, such as PZT, have a high power density, high bandwidth, and high efficiency. PZT outperforms other actuator materials, including shape memory alloy (SMA), conducting polymers, and electostrictive elastomers, with respect to speed of response and bandwidth. Its maximum stress is as large as SMA, and the efficiency is comparable to electrostrictive elastomers.

The most critical drawback of PZT is its extremely small strain, i.e., only 0.1%. Over the last several decades efforts have been taken to generate displacements out of PZT that are large enough to drive robotic and mechatronics systems [1] [2] [3] [4] [5] [6] [7] [8] [9] [10] [11] [12]. These can be classified into a) inching motion or periodic wave generation, b) bimetal-type bending, c) leverage-type motion amplification, and d) flextensional mechanisms. Inching motion entails friction drive, which limits its applicability to a class of applications. Bimetal-type mechanisms [11] can produce only small forces despite their large displacement and strain, which also limit applications to small loads. Leverage-type motion amplification [8] is inefficient, producing only a marginal gain on the order of 10. It tends to be bulky and heavy if several leverages are connected to produce a larger displacement. A wide variety of flextensional mechanisms has been studied and developed such as "Moonie" [1] [4], "Cymbal" [7], "Rainbow" [3], and others [9]. An individual actuator, such as C-block [5] and Moonie [4], can be stacked in series to increase the total displacement. However, this stacking also increase the size of overall mechanism and does not improve the strain itself, which is known to be up to 2–3%, e.g., by flextensional mechanisms. Therefore, a more compact actuator with larger strain is considered necessary for driving a wide variety of mechatronic systems.

The new "nested rhombus" approach we have proposed [13] is particularly useful for gaining a large strain in a compact body, appropriate for many applications. A large amplification gain on the order of several hundreds can be obtained with this method. Although the original strain of PZT stacks is only 0.1%, the resultant nominal strain of the new actuator is over 20%. The key idea of this large strain amplification is hierarchical nested architecture. Strain is amplified α times at each layer of the hierarchical structure. Unlike traditional leverage mechanisms, where the gain α is proportional to the dimension of the lever or number of stacks, the amplification gain of the new mechanism increases exponentially as the number of layers increases. For K layers of hierarchical mechanism, the resultant gain is given by α^K , the power of the number of layers. This nesting method allows us to gain a large strain in a compact body. Therefore, the actuator is suitable for the cellular actuator concept [14].

This paper proposes a static lumped parameter model for the design and analysis of nested PZT cellular actuators with exponential strain amplification mechanisms. A kinematic and static model including mechanical compliance of the nested strain amplifier will be developed to investigate how the forces and displacements generated by the individual PZT actuators are transmitted through the hierarchical mechanism, resulting in aggregate force and displacement at the output node. Design trade-offs will be discussed based on the model. The validity of the proposed concept will be confirmed through the design of a prototype actuator having 21% effective strain, 1.7N blocking force, and 15g of body mass.

II. Nested Rhombus Structure

Several amplification mechanisms for amplifying small displacements of PZT actuators have already been developed both in macro [1] and micro scale [12] and have been used for commercial products by [15]. Our technique based on the traditional "Moonie" mechanism [1] extends the strain amplification exponentially with use of a nested structure. As shown in Fig. 1, the basic part of the mechanism is a rhombus-like hexagon that contracts vertically as the internal unit shown in grey expands. Assume that the beams of

J. Ueda, T. Secord, and H. H. Asada are with the Department of Mechanical Engineering, Massachusetts Institute of Technology, Cambridge, MA, USA.{uedajun,secord,asada@mit.edu}

J. Ueda is also with the Graduate School of Information Science, Nara Institute of Science and Technology, Ikoma, Nara, Japan.

the rhombus are completely rigid and that all the joints are free to rotate and purely revolving. As a result, the vertical displacement, that is, the output of the mechanism, is amplified.

Our method is to extend this technique to:

1) Gain an order-of-magnitude larger strain amplification, and
2) Build a modular structure that is flexible and extensible.

Figure 2 illustrates a new mechanism, called a "nested rhombus" strain amplifier, which consists of the multitude of rhombus mechanisms arranged in a hierarchical structure. The inner-most unit, i.e. the building block of the hierarchical system, is the standard rhombus mechanism described above. These units are connected in series to increase the output displacement. Also these units can be arranged in parallel to increase the output force. The salient feature of this hierarchical mechanism is that these rhombus units are enclosed with a larger rhombus mechanism that amplifies the total displacement of the smaller rhombus units. These larger rhombus units are connected together and enclosed with an even larger rhombus structure to further amplify the total displacement. As this enclosure and amplification process is repeated, a multi-layer strain-amplification mechanism is constructed, and the resultant displacement increases exponentially.

This nested rhombus mechanism has a number of variations, depending on the numbers of serial and parallel units arranged in each layer and the effective gain in each layer. Let K be the number of amplification layers. In general the resultant amplification gain is given by the multiplication of each layer gain:

$$\alpha_{total} = \prod_{k=1}^{K} \alpha_k. \tag{1}$$

where α_k is the k-th layer's effective gain of strain amplification. Put more simply, assuming that each layer amplifies the strain α times, the resultant amplification gain is given by α to the *power* of K:

$$\alpha_{total} = \alpha^K. \tag{2}$$

The nested rhombus mechanism with this hierarchical structure is a powerful tool for gaining an order-of-magnitude larger amplification of displacement. For $\alpha = 15$ the gain becomes $\alpha_{total} = 225$ by nesting two rhombus layers, leading to over 20% effective strain: $\alpha = 15$ and $K = 2$: $0.1\% \times 15 \times 15 = 22.5\%$, which is comparable to natural skeletal muscles.

Another important feature of the nested rhombus mechanism is that two planes of rhombi in different layers may be arranged perpendicular to each other. Three-dimensional arrangement of nested rhombus mechanisms allows us to densely enclose many rhombus units in a limited space. For example, Figure 2 illustrates a 3-dimensional structure. Note that the serially connected first-layer rhombus units are rotated 90 degrees about their output axis x_1. This makes

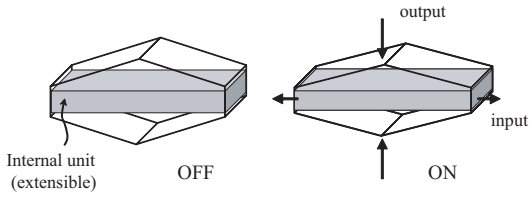

Fig. 1. Strain Amplification by Ideal Rhombus Mechanism

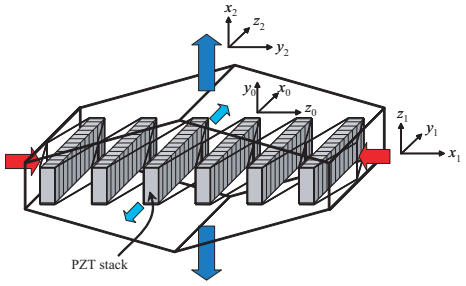

Fig. 2. 3 Dimensional Nested Rhombus Mechanism for over 20% Effective Strain [13]

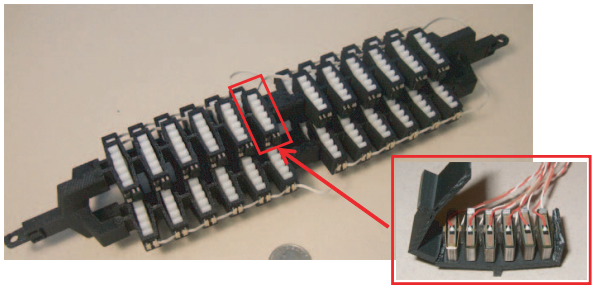

Fig. 3. Cellular Actuators: 12 stacks and 4 bundles (Mock-up)

the rhombus mechanism at the second layer more compact; the length in the x_2 direction is reduced.

Furthermore, it should be noted that diverse configurations can be made simply by changing the serial and parallel arrangements of the same building blocks. Figure 3 shows an example configuration where 12 units shown in Fig. 2 are connected in series and 4 arrays are connected in parallel. This modular design is a powerful method for building diverse actuators with matched load impedance, stroke, and force requirements.

III. Effects of Joint Stiffness and Beam Compliance

The initial design [13] has been presented to show the potential of the nested Rhombus PZT actuator to produce an effective strain of 20% based on the ideal kinematic model having rigid beams and free joints at the strain amplification mechanism. Actual mechanisms, however, inevitably have some compliance at the structure. Such a structural compliance has a significant influence upon the aggregate force and displacement. Care must be taken in designing the nested strain amplification mechanism, since intricate interplays between the structural stiffness and the inherent stiffness of the PZT stack actuator exist in the system.

Note that fabrication of free joints is difficult in small scale due to mechanical tolerance and play. For the first and second layers, in particular, where the displacement is extremely small, the displacement created by the PZT is likely to diminish due to play at the joints. Therefore, flexural pivots and flexible beams [9] [12] [15] have been used for amplifying PZT displacement. Figure 4 shows an example embodiment of the rhombus mechanism. These flexural joints and beams inevitably bring undesirable properties to the system. There are three types of undesirable properties:

1). First, the joints are no longer free joints, but they impose a spring load that the PZT has to overcome. Some fraction of the PZT force is wasted for coping with the joint stiffness. This results in reduction in free-load displacement. This implies that the joint stiffness has an equivalent effect to that of the internal PZT stiffness. The stiffness of the joints brings increased stiffness for the PZT to overcome.

2). Second, flexibility at the beams may attenuate the displacement and force created by the PZT. As the PZT generates a displacement, the beams are deformed and thereby the transmitted force becomes lower; at least it does not reach the same level as that of the rigid beams. Similarly, if the output axis is coupled to another compliant load, the output force and displacement will be prorated between the load compliance and the beam compliance. As the beam stiffness becomes lower, the output force and displacement decrease.

3). Third, flexural joints not only create pure rotational displacements but also often cause unwanted translational displacements. These elastic deformations at the joint along the direction of the beam incur the same problem as the beam compliance; the force and displacement created by the PZT tend to diminish at the joints.

It is important to distinguish two different types of compliance in the above cases: One is to take place in the kinematically admissible space of the ideal rhombus mechanism, and the other is in the orthogonal complement to the former, termed the constrained space. The joint stiffness described in 1) is in the admissible motion space, while 2) and 3) are in the constrained space. Curved beams, such as seen in Moonies, contain compliance in both constrained and admissible spaces. The distributed compliance can be approximated into the two types of lumped compliant elements. To minimize the adverse effects of the nested rhombus mechanism, the stiffness in the admissible space must be minimized and the stiffness in the constrained space must be maximized. As multiple layers of strain amplification mechanisms are used, the compliances in the admissible and constrained spaces become more intricate.

IV. Nested Rhombus Mechanisms with Structure Flexibility

A. Modeling of Single-Layer Flexible Rhombus Mechanisms

Consider the case shown in Fig. 5 (a) where a rhombus mechanism, including Moonies, is connected to a spring load. k_{load} is an elastic modulus of the load, and k_{pzt} is an elastic modulus of the internal unit such as a PZT stack actuator. Δx_{pzt} is the displacement of the internal unit, and

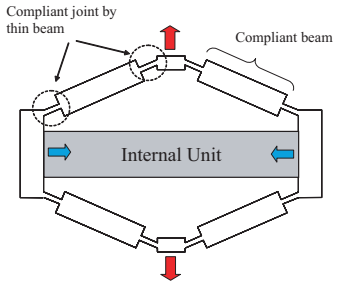

Fig. 4. Embodiment of Rhombus Mechanism

f_{pzt} is the force applied to the amplification mechanism from the internal unit. f_1 is the force applied to the load from the actuator, and Δx_1 is the displacement of the load. In this figure, we assume that the internal unit is contractive for later convenience. Only the static case is considered for modeling; the effect of the distribution of mass and damper is neglected.

The rhombus strain amplification mechanism is a two-port compliance element, whose constitutive law is given by a 2x2 stiffness matrix defined as:

$$\begin{bmatrix} f_I \\ f_O \end{bmatrix} = \boldsymbol{S} \begin{bmatrix} \Delta x_{pzt} \\ \Delta x_1 \end{bmatrix} \tag{3}$$

where $S^{2\times 2} = \begin{bmatrix} s_1 & s_3 \\ s_3 & s_2 \end{bmatrix}$ is a stiffness matrix. f_I is the net force applied to the mechanism from the internal unit, and f_O is the reaction force from the external load. Note that the stiffness matrix $\boldsymbol{S}$ is non-singular, symmetric, and positive-definite; $s_1 > 0$, $s_2 > 0$ and $s_1 s_2 - s_3^2 > 0$. The symmetric nature of the stiffness matrix follows Castigliano's theorems. When the input port of this mechanism is connected to a PZT stack actuator producing force f_{pzt} with inherent stiffness k_{pzt} and the output port is connected to a load of stiffness k_{load}, we have

$$f_I = f_{pzt} - k_{pzt}\Delta x_{pzt} = s_1 \Delta x_{pzt} + s_3 \Delta x_1 \tag{4}$$

$$f_O = -f_1 = -k_{load}\Delta x_1 = s_3 \Delta x_{pzt} + s_2 \Delta x_1. \tag{5}$$

Eliminating Δx_{pzt} from the above equations yields:

$$f_{pzt} = -\left(\frac{k_{pzt} + s_1}{s_3} k_{load} + \frac{s_2(k_{pzt} + s_1) - s_3^2}{s_3} \right) \Delta x_1 \tag{6}$$

Defining

$$\tilde{f} \triangleq \frac{-s_3}{k_{pzt} + s_1} f_{pzt} \tag{7}$$

$$\tilde{k} \triangleq \frac{s_2(k_{pzt} + s_1) - s_3^2}{k_{pzt} + s_1} = \frac{s_2 k_{pzt} + \det \boldsymbol{S}}{k_{pzt} + s_1} > 0, \tag{8}$$

the above equation (6) reduces to

$$\tilde{f} = (k_{load} + \tilde{k}) \Delta x_1 \tag{9}$$

Force $\tilde{f}$ and stiffness $\tilde{k}$ represent the effective PZT force and the resultant stiffness of the PZT stack all viewed from the output port of the amplification mechanism.

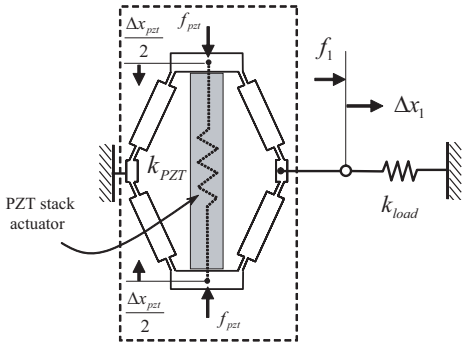

(a) Rhombus Mechanism with Structural Flexibilities

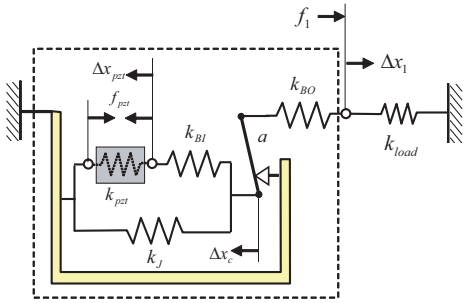

(b) Lumped Parameter Model

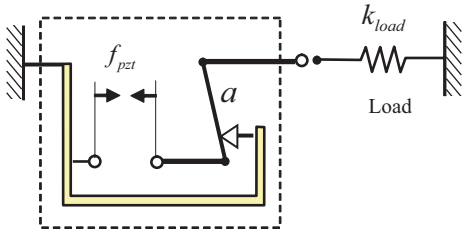

(c) Model of Idealized Rhombus ($k_{BI}, k_{BO} \to \infty$, $k_J \to 0$)

Fig. 5. Model of Rhombus Mechanism with Flexibility

A drawback with the above two-port model representation is that it is difficult to gain physical insights as to which elements degrade actuator performance and how to improve it through design. In the previous section two distinct compliances were introduced, one in the admissible motion space and the other in the constrained space. To improve performance with respect to output force and displacement, the stiffness in the admissible motion space must be minimized, while the one in the constrained space must be maximized. To manifest these structural compliances, consider a lumped parameter model shown in Fig. 5 (b) with 3 spring elements, k_J, k_{BI} and k_{BO}, and one amplification leverage a. As the spring constants, k_{BI} and k_{BO}, tend to infinity, the system reduces to the one consisting of all rigid links, where the output Δx_1 is directly proportional to the input displacement Δx_{pzt}. Stiffness k_J impedes this rigid body motion, representing the stiffness in the admissible motion space. Elastic deformation at k_{BI} and k_{BO} represent deviation from the rigid body motion.

From Figure 5 (b),

$$f_{pzt} + k_{BI}(\Delta x_c - \Delta x_{pzt}) - k_{pzt}\Delta x_{pzt} = 0 \quad (10)$$

$$a \cdot k_{BO}(a \cdot \Delta x_c - \Delta x_1) + k_J \Delta x_c + k_{BI}(\Delta x_c - \Delta x_{pzt}) = 0 \quad (11)$$

$$f_1 = k_{load}\Delta x_1 = k_{BO}(a \cdot \Delta x_c - \Delta x_1), \quad (12)$$

where Δx_c is the displacement at the connecting point between the leverage and springs; however this point is virtual and Δx_c does not correspond to a physical displacement. This model is applicable to a wide variety of "rhombus-type" amplification mechanisms including Moonies.

Consider the blocking force when the PZT stack actuator generates its maximum force, $f_{pzt\,\max}$, given as follows:

$$f_1^{block} = \frac{a k_{BI} k_{BO}}{(a^2 k_{BI} k_{BO} + k_{BI} k_J) + k_{pzt}(a^2 k_{BO} + k_J + k_{BI})} f_{pzt\,\max}. \quad (13)$$

Similarly, the free-load displacement for this rhombus mechanism, where $k_{load} \to 0$, is given by

$$\Delta x_1^{free} = \frac{a k_{BI}}{k_{pzt}(k_{BI} + k_J) + k_J k_{BI}} f_{pzt\,\max}. \quad (14)$$

As addressed above, these equations imply that the blocking force will be maximized by $k_{BI}, k_{BO} \to \infty$. Similarly, $k_J \to 0$ maximizes Δx_1^{free}. The other advantage is that the 3-spring model is able to represent the ideal rhombus as a special case as shown in Fig. 5 (c).

B. Model Simplification

From (10) to (12), the relationship between f_{pzt} and Δx_1 is given by

$$\begin{aligned}(a\, k_{BI} k_{BO}) f_{pzt} = \\ \big[k_{load}\{a^2 k_{BI} k_{BO} + k_{BI} k_J + k_{pzt}(a^2 k_{BO} + k_J + k_{BI})\} \\ + k_{BO}(k_{BI} k_J + k_{pzt} k_J + k_{BI} k_{pzt})\big]\, \Delta x_1. \end{aligned} \quad (15)$$

The above equation can be written as

$$\tilde{f}_1 = (k_{load} + \tilde{k}_1)\Delta x_1 \quad (16)$$

where

$$\tilde{k}_1 \triangleq \frac{k_{BO}(k_{BI} k_J + k_{pzt} k_J + k_{BI} k_{pzt})}{(a^2 k_{BI} k_{BO} + k_{BI} k_J) + k_{pzt}(a^2 k_{BO} + k_J + k_{BI})} \quad (17)$$

$$\tilde{f}_1 \triangleq \frac{a k_{BI} k_{BO}}{(a^2 k_{BI} k_{BO} + k_{BI} k_J) + k_{pzt}(a^2 k_{BO} + k_J + k_{BI})} f_{pzt}. \quad (18)$$

This implies that the proposed lumped parameter model can be further simplified. As will be described in the following section, this simplification enables performance evaluation for complex nested mechanisms simply by nesting a simplified model of lower layers into a lumped parameter model. As a result, the performance of the overall mechanism such as aggregate displacement and force can be predicted in a recursive manner.

C. Recursive Formula of Aggregate Force and Displacement of Flexible Nested Mechanisms

The goal of this section is to describe a recursive formula to obtain an equivalent model for a general nested mechanism. Figure 6 shows a nested rhombus structure. As addressed in the previous sections, each nested layer can be represented by its equivalent model, which enables us to describe the force-displacement property for the nested structure in an iterative manner. Let K be the number of nesting layers. Also, let k_{Jk}, k_{BIk}, k_{BOk}, N_k be the joint

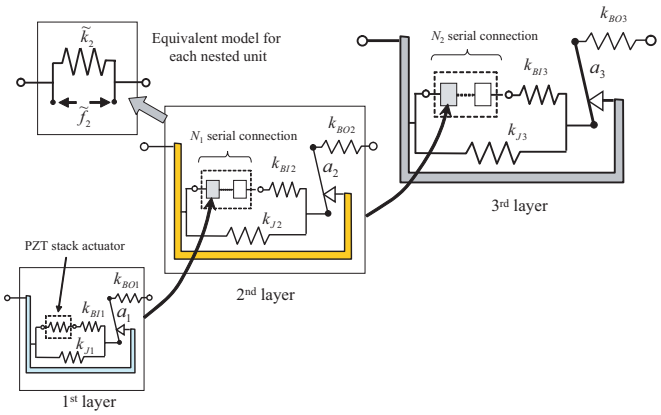

Fig. 6. Recursive Formula for Nested Rhombus Model

compliance, beam compliances, and the number of serial connection for the k-th ($k = 1, \cdots K$) layer. This mechanism involves $N_{K-1} \cdot N_{K-2} \cdots N_1$ PZT stack actuators.

By applying (17) and (18), the equivalent model for the k-th layer can be represented by

$$\tilde{k}_k = \frac{k_{BOk}(k_{BIk}k_{Jk} + \frac{\tilde{k}_{k-1}}{N_{k-1}}k_{Jk} + k_{BIk}k_{pzt\ k})}{(a_k^2 k_{BIk}k_{BOk} + k_{BIk}k_{Jk}) + \frac{\tilde{k}_{k-1}}{N_{k-1}}(a_k^2 k_{BOk} + k_{Jk} + k_{BIk})} \quad (19)$$

$$\tilde{f}_k = \frac{a_k k_{BIk} k_{BOk}}{(a_k^2 k_{BIk}k_{BOk} + k_{BIk}k_{Jk}) + \frac{\tilde{k}_{k-1}}{N_{k-1}}(a_k^2 k_{BOk} + k_{Jk} + k_{BIk})} \times \frac{1}{N_{k-1}} \sum_{i=1}^{N_{k-1}} \tilde{f}_{k-1}^i, \quad (20)$$

where $\tilde{f}_{k-1}^i$ is the equivalent force of the i-th unit in the $(k-1)$-th layer.

V. Prototype Actuator

A. Mechanical Design of Rhombus Mechanism

A prototype nested actuator with over 20% effective strain is designed based on the structural compliance analysis. Consider a nested structure with 2 amplification layers as shown in Fig. 2. The APA50XS "Moonie" piezoelectric actuators developed by Cedrat Inc. [15] are adopted for the first layer. According to the preliminary design in Fig. 2, over 20% of effective strain can be obtained by a two-layer mechanism. By stacking 6 APA50XS actuators for the first layer, i.e., $N_1 = 6$, this large strain may be achieved with a proper design of the second layer. From Table I, we have $\tilde{k}_1$=0.225 $\times 10^6$ [N/m], and $\tilde{f}_1^{block}$=18.0 [N] for the first layer units. The remainder of this section focuses on the design of the second-layer rhombus mechanism.

From (19) and (20) we obtain an equivalent model for the second layer by substituting (17) and (18), which provides a design guideline in terms of k_{BI2}, k_{BO2} and k_{J2} for the target effective strain, i.e., 20%. As described in the previous section, the stiffness in the admissible space, i.e., k_{J2}, must be minimized. In addition, in order to increase the stiffness

TABLE I

Characteristics of the APA50XS Actuator [15] for the First Layer(definition of the dimensions has been modified.)

Displacement	80 [μm]
Blocking Force $\tilde{f}_1^{block}$	18.0 [N]
Stiffness $\tilde{k}_1$	0.225 [N/μm]
Voltage range	-20 – 150 [V]
Length (output actuation direction)	4.7 [mm]
Width (pzt stack actuation direction)	12.8 [mm]
Height	9.0 [mm]
Mass	2.0 [g]

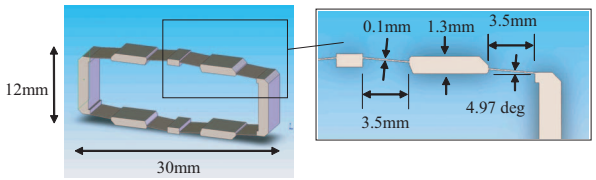

Fig. 7. Design of Rhombus Mechanism for the 2nd Layer

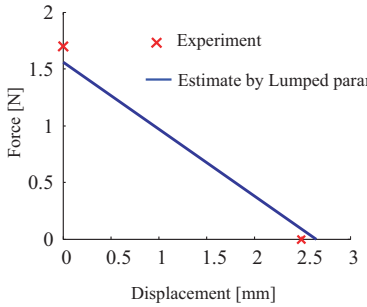

Fig. 8. Force and Displacement Property of Prototype Actuator

in the constrained space, i.e., k_{BI2} and k_{BO2}, the oblique beam need to have a sufficient thickness except the thin part for the compliant joint.

Figure 7 shows the designed rhombus mechanism for the second layer. Phosphor bronze (C54400, H08) is used for the material. The length of the mechanism in actuation direction is 12 [mm], and the width is 30 [mm]. The thickness of 0.1 [mm] is given to thin sections that work as compliant joints considering electrical discharge machining. The thickness of 1.3 [mm] is given to the oblique beams for sufficient stiffness. The oblique angle of the beams is 4.97 [deg] that gives the displacement amplification ratio of 11.5 assuming the mechanism is ideal.

The lumped parameters are calibrated as $\hat{k}_{BI2} = 6.72 \times 10^6$ [N/m], $\hat{k}_{BO2} = 5.21 \times 10^4$ [N/m], $\hat{k}_{J2} = 3.98 \times 10^4$ [N/m], and $\hat{a}_2 = 11.4$. Figure 8 shows the estimated force and displacement property of the prototype actuator. The analysis predicts that the maximum free-load displacement is 2.64 [mm], which is equivalent to 22% effective strain.

B. Development and Performance Evaluation

Figure 9 shows the assembled actuator with 6 first-layer units. The second layer mechanism weighs approximately 3 [g], resulting in the total weight of 15 [g]. Figure 10

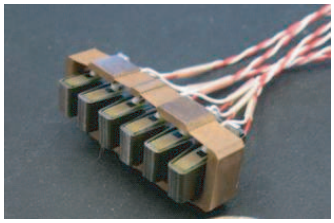

Fig. 9. Prototype Actuator

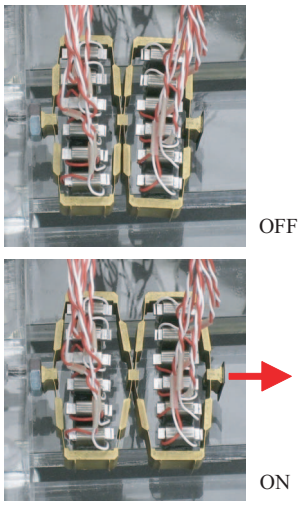

Fig. 10. Snapshots of Free-load Displacement: Two Nested Rhombus Mechanisms are Connected in Series.

shows snapshots of free-load displacement where 2 rhombus mechanisms are connected in series. This actuator extends since the first layer units are contractive.

The performance of this prototype is evaluated by measuring free-load displacement and blocking force. Figure 11 (a) shows the maximum free-load displacement measured using a laser displacement sensor (Micro-Epsilon optoNCDT 1401) when all 6 units are ON by applying 150 [V] actuation voltage. The measured displacement is 2.49 [mm] that is equivalent to 20.8% effective strain. Figure 11 (b) shows the blocking force where a sinusoidal wave input ranging from 0 –150 [V] is applied. The maximum blocking force measured using a compact load cell (Transducer Techniques MLP) is 1.7 [N]. As shown in Fig. 8, the estimated values by using the lumped parameter model agree well with the experiment, which confirms the validity of the approach.

VI. Conclusions and Future Works

In this paper, a static lumped parameter model for the nested PZT cellular actuators with exponential strain amplification mechanisms has been presented. Based on this model, a prototype actuator system having 21% effective strain, 1.7N blocking force, and 15g of body mass has been designed. Future work includes (1) dynamic modeling to quantify high frequency response, (2) analysis of a closed kinematic chain formed by serial/parallel mixed configuration, (3) application to robotic systems. The first author gratefully expresses his

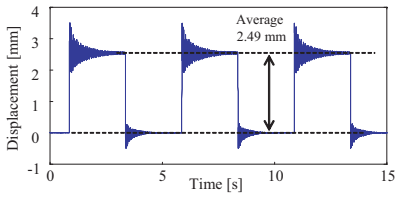

(a) Free-load Displacement: Step response

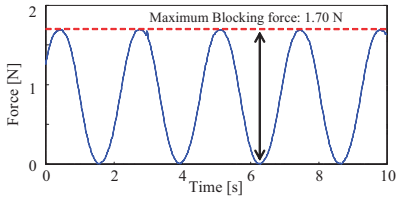

(b) Blocking-force: Sinusoidal wave input

Fig. 11. Experimental Result

thanks to the Japan Society for the Promotion of Science. This work is supported by Sumitomo Heavy Industries, Ltd.

References

[1] R. Newnham, A. Dogan, Q. Xu, K. Onitsuka, J. Tressler, and S. Yoshikawa, "Flextensional moonie actuators," in *1993 IEEE Proceedings. Ultrasonics Symposium*, vol. 1, Oct.31- Nov. 3 1993, pp. 509–513.

[2] A. Dogan, Q. Xu, K. Onitsuka, S. Yoshikawa, K. Uchino, and R. Newnham, "High displacement ceramic metal composite actuators (moonies)," *Ferroelectrics*, vol. 156, no. 1, pp. 1–6, 1994.

[3] G. Haertling, "Rainbow Ceramics- A new type of ultra-high-displacement actuator," *American Ceramic Society Bulletin*, vol. 73, no. 1, pp. 93–96, 1994.

[4] K. Onitsuka, A. Dogan, J. Tressler, Q. Xu, S. Yoshikawa, and R. Newnham, "Metal-ceramic composite transducer, the "moonie"," *Journal of Intelligent Material Systems and Structures*, vol. 6, no. 4, pp. 447–455, 1995.

[5] A. Moskalik and D. Brei, "Quasi-Static Behavior of Individual C-Block Piezoelectric Actuators," *Journal of Intelligent Material Systems and Structures*, vol. 8, no. 7, pp. 571–587, 1997.

[6] K. Uchino, *Piezoelectric Actuators and Ultrasonic Motors*. Kluwer Academic Publishers, 1997.

[7] A. Dogan, K. Uchino, and R. Newnham, "Composite piezoelectric transducer with truncated conical endcaps "cymbal"," *Ultrasonics, Ferroelectrics and Frequency Control, IEEE Transactions on*, vol. 44, no. 3, pp. 597–605, May 1997.

[8] "Lever actuator comprising a longitudinal-effect electroexpansive transducer," US Patent 4,435,666.

[9] P. Janker, M. Christmann, F. Hermle, T. Lorkowski, and S. Storm, "Mechatronics Using Piezoelectric Actuators," *Journal of the European Ceramics Society*, vol. 19, no. 6, pp. 1127–1131, 1999.

[10] C. Niezrecki, D. Brei, S. Balakrishnan, and A. Moskalik, "Piezoelectric actuation: State of the art," *The Shock and Vibration Digest*, vol. 33, no. 4, pp. 269–280, 2001.

[11] K. Seffen and E. Toews, "Hyperhelical Actuators: Coils and Coiled-Coils," in *45th AIAA/ASME/ASCE/AHS/ASC Structures, Structural Dynamics and Materials Conference*, April 2004, pp. 19–22.

[12] N. Conway, Z. Traina, and S. Kim, "A strain amplifying piezoelectric MEMS actuator," *Journal of Micromechanics and Microengineering*, vol. 17, no. 4, pp. 781–787, 2007.

[13] J. Ueda, T. Secord, and H. H. Asada, "Design of pzt cellular actuators with power-law strain amplification," in *Intelligent Robots and Systems, 2007. IROS 2007. IEEE/RSJ International Conference on*, Oct. 29 2007-Nov. 2 2007, pp. 1160–1165.

[14] J. Ueda, L. Odhner, and H. H. Asada, "Broadcast Feedback of Stochastic Cellular Actuators Inspired by Biological Muscle Control," *The International Journal of Robotics Research*, vol. 26, no. 11-12, pp. 1251–1265, 2007.

[15] CEDRAT Inc., http://www.cedrat.com/.